Journal of Materials Processing Tech. 305 (2022) 117599

Contents lists available at ScienceDirect

Journal of Materials Processing Tech.

journal homepage: www.elsevier.com/locate/jmatprotec

Mechanism study of electropolishing from the perspective of etching isotropy

Rong Yi, Jianwei Ji, Zejin Zhan, Hui Deng *

Department of Mechanical and Energy Engineering, Southern University of Science and Technology, No. 1088, Xueyuan Road, Shenzhen, Guangdong 518055, China

ARTICLE INFO

Associate Editor: Adam Thomas Clare

Keywords:
Electropolishing
Etching isotropy
Electrochemical etching
Roughness

ABSTRACT

Electropolishing, as a damage-free and highly efficient surface finishing method, has been widely used for finishing of metal components. In this study, the electropolishing mechanism of tungsten in the electrolyte with H_2SO_4 and CH_3OH was investigated from the perspective of etching isotropy. The anodic dissolution behavior of tungsten demonstrated that anisotropic and isotropic etching occurred under the activation polarization and mass transfer polarization, respectively. The evolution of surface morphology, roughness, and electric current density during electropolishing has been experimentally investigated and analyzed. According to the changes in surface morphology and current density, there was a transformation from anisotropic etching to isotropic etching during the electropolishing due to the time-consuming accumulation of reactive products. The application of a pulse power supply with a duty cycle of 10% resulted in a rough surface on tungsten due to the mass transfer polarization being inhibited. Similar results were also obtained in the electrolyte with 2 wt% NaOH. The presented findings experimentally demonstrate the importance of the isotropic etching mode for electropolishing, which is of great value for further revealing the electropolishing mechanism.

1. Introduction

As the metal with the highest melting point (3410 ℃), tungsten plays an important role in commercial, industrial, and military applications due to its excellent physical and chemical properties (Tomashov and Chernova, 1967). At the beginning of the 20th century, tungsten metal was only used as a filament in incandescent light bulbs and as an alloying element in steel, however, as mentioned by Sachs (1999), today it is very common and covers different fields such as electrical contacts, electron emitter, welding electrodes, etc. After the introduction of scanning tunneling microscopy (STM) and atomic force microscopy, another important application of tungsten is in the manufacture of scanning probes as discussed by Ionov et al. (2020). Furthermore, Philipps (2011) and Rieth et al. (2013) respectively suggested that tungsten is a promising material for plasma-facing components and helium-cooled divertor in fusion power reactor, due to its nano-manufacturing and metrology high-temperature strength, and high plasma sputtering erosion resistance.

However, the low ductility at room temperature and high ductile-brittle transition temperature of tungsten causes serious challenges to its machinability as Ren et al. (2018) mentioned. According to Suzuki et al. (2007), even ultra-precision diamond cutting is not applicable, due to the adhesion of the tungsten material to the tool, the rapid tool wear, and the brittle fracture. Although diamonds are considered as an integral tool material in ultra-precision machining and commonly used in the ultra-precision cutting of non-ferrous, electroless nickel, and optical crystals, as mentioned by Jiang et al. (2020). Therefore, Chen et al. (2010) suggested that wire electrical discharge machining (WEDM) is an important non-traditional machining process for tungsten. During the WEDM, the material is eroded from the workpiece by a series of discrete sparks between the workpiece and the wire electrode, as discussed by Puri and Bhattacharyya (2003). According to Aspinwall et al. (2008), the thermal character of WEDM induces a resolidified zone and a heat affected zone on the machined surface, which can degrade the surface roughness and integrity of the machined part. Therefore, post processing to remove the recast layers is required, especially in mold applications where a smooth surface with no subsurface damage is essential for good form accuracy as Wang et al. (2014) mentioned.

As a highly efficient and free of mechanical interaction polishing technique, Landolt et al. (2003) implied that electropolishing is a promising approach to polishing metal parts. So far, electropolishing has been widely used in the surface treatment of metallic materials.

* Corresponding author.
E-mail address: dengh@sustech.edu.cn (H. Deng).

https://doi.org/10.1016/j.jmatprotec.2022.117599
Received 22 February 2022; Received in revised form 6 April 2022; Accepted 10 April 2022
Available online 13 April 2022
0924-0136/© 2022 Elsevier B.V. All rights reserved.

Neelakantan and Hassel (2008) studied the electropolishing of NiTi in electrolytes with methanol and sulfuric acid. Di et al. (2009) investigated the electropolishing of high-purity aluminum in perchloric acid and ethanol solutions. Han and Fang (2020a) found that eco-friendly NaCl-based electrolyte is suitable for electropolishing 316 L stainless steel. During electropolishing, the workpiece to be polished works as an anode, and connects with the positive electrode of a DC power. The anode metal is oxidized into metal ions due to the loss of electrons. Then, it dissolves into the electrolyte, resulting in the removal of surface materials, and the surface becomes smooth under optimized conditions. According to Yang et al. (2017), electropolishing offers many advantages over other surface smoothing processes. Since the aqueous electrolyte is used as the polishing media, electropolishing could be used to polish complex-shaped parts, as mentioned by Ferchow et al. (2020); According to Wynick and Boehlert (2005), as there is no mechanical interaction in electropolishing, no mechanical damage or residual stress is left after polishing.

Although electropolishing has been used for decades, its mechanism has not been fully understood yet. Considering that oxidation, dissolution, and diffusion simultaneously occur in the electropolishing process, mass transfer has always been considered an important process. According to the difference of the rate limited process, there are three mass transport mechanisms as summarized by Landolt (1987): the dissolved metal cations diffusion control theory, the acceptor anions diffusion control theory (Matlosz et al., 1994), and the water diffusion control theory (Magaino et al., 1993).

A variety of mechanisms of electropolishing were proposed based on the mass transfer process. Jacquet (1935) proposed the viscous film theory which has been most widely accepted. A viscous liquid film composed of dissolved oxidation products with high viscosity and large electrical resistance is formed on the workpiece surface. The thickness of the viscous liquid film is not uniform along the rough surface and the thickness at the depressed parts is greater than that at the raised parts. Therefore, the dissolution of the raised parts is relatively fast, and the result is that the rough surface is macroscopically polished. Wang et al. (2019) suggested that the electropolishing of tungsten is controlled by the viscous film composed of WO^{4-}. Elmore (1939) developed the diffusion theory later for electropolishing of copper in the orthophosphoric system. Since the concentration gradient of dissolved metal ions around the raised part is lower, its dissolution is promoted and results in the effect of polishing. Based on these theories, Halfawy (1951) suggested the importance of anion diffusion on the surface of the anode for metal electropolishing and proposed the acceptor theory. Based on this theory, the dissolution and polishing of the metal were attributed to the anions along the anodic surface. Hoar et al. (1965) proposed a passivation theory, a very thin passive film is formed on the anode surface, the inconsistent thickness of the passivation layer along with the rough surface results in the polishing effect of the surface.

Different from the aforementioned theories, Yi et al. (2020) et al. proposed a generic isotropic etching polishing (IEP) mechanism based on the surface topography evolution under mass transfer polarization. In IEP, due to the formation of an oxide film on the metal surface, the etching occurred preferably at the weak sites of the metal surface as the DC power was applied. Since the dissolution of metal is controlled under mass transfer polarization, the shape of those etching pits was hemispherical. As the etching duration increases, the neighboring etching pits start to merge. Finally, the entire rough surface is completely replaced by the smooth inner surface of the merged hemispherical etching holes, and then a smooth surface is obtained. As a generic approach, IEP allows the polishing of different metals while using the same polishing solution. The wet grounded surface of IN718 was transformed into a mirror-like smooth surface after 300 s of IEP at optimized conditions, as Muhammad Ajmal et al. (2021) demonstrated.

In the present research, the electropolishing mechanism of tungsten was investigated from the perspective of isotropic etching. The polarization curve and chronoamperometry were used to investigate the etching mode of tungsten under activation polarization and mass transfer polarization. The surface topography evolution during the dissolution of tungsten was studied to explore the electropolishing process. In addition, the influence of oxide film, pulse power supply, and electrolyte composition on the electropolishing process were analyzed.

2. Experimental approach

Commercially available pure tungsten substrates with a diameter of 15 mm and thickness of 3 mm were utilized in this study. The face towards the anode was processed by electropolishing while the side and back faces were covered by Teflon. The substrates were lapped by SiC sandpapers (#500) to remove the rough cutting marks introduced by wire cut. Then the substrates were ultrasonically cleaned in deionized water and ethyl alcohol for 5 min respectively to remove contaminants. Before the experiments, all the substrates were electropolished in the electrolyte with 0.5 wt% NaOH for an hour at the voltage of 10 V to remove the sub-surface damage.

Electrochemical properties were measured using an electrochemical workstation (CHI660e, Shanghai Chenhua Instrument Co., LTD). Thermal oxidation experiments were carried out in a tube furnace (OFT-1200X, Hefei Kojing Material Technology Co., LTD). A multifunction generator (WF1973, Keysight Technologies) and a high-speed bipolar amplifier (HAS 4052, Keysight Technologies) were used as a pulse power supply. KEITHLEY 2280S was used as a DC power supply. A glass beaker containing electrolyte was used as the reaction cell. A platinum mesh (2 cm × 2 cm) connected to the negative electrode of a DC power worked as the cathode. The substrate worked as the anode and was connected to the positive electrode of the DC power. The distance between the cathode and anode was kept at 60 mm. The current and voltage were recorded during the experiment and exported to a connected computer. After polishing, the substrates were cleaned in deionized water before characterization. Without special instructions, all the experiments were carried out at room temperature.

Two electrolytes were used: the H_2SO_4 electrolyte was composed of analytical grade sulfuric acid (97%) and methanol (99.5%), while the NaOH electrolyte was composed of NaOH and distilled water. On the workpiece surface which is considered as the anode, an oxidation reaction occurs, and then the oxide is dissolved into the electrolyte. Meanwhile, a reduction reaction occurs around the cathode. The reactions occurring on the cathode and anode are listed as follows (O refers to the oxide in the electrolyte, and R refers to the reduction product):

$$\text{Cathode}: \quad O + ne^- \rightarrow R \tag{1}$$

$$\text{Anode}: M(s) \rightarrow M^{n+} + ne^- \tag{2}$$

Before and after polishing, the surface morphology was examined by scanning electron microscopy (SEM, ZEISS Merlin), and surface roughness was measured by atomic force microscopy (AFM, Bruker Edge), and the surface roughness was measured by scanning white light interferometer (Taylor Hobson M112-4449-02 CCI HD).

3. Results and discussion

3.1. Anodic dissolution behavior

As a preliminary investigation, the polarization curve of tungsten was measured. Fig. 1(a) shows the polarization curve of tungsten in the electrolyte with a 15:100 volume ratio of H_2SO_4 to CH_3OH. In the anodic polarization region, the curve was divided into two regions. In the voltage range from − 0.1 to 4.8 V, the current density increased with the voltage, indicating the overpotential serves to provide the activation energy required to drive the dissolution process, as discussed by Bard and Faulkner (2002). In other words, the dissolution of tungsten is activation polarization. In this region, the dissolution rate of crystal

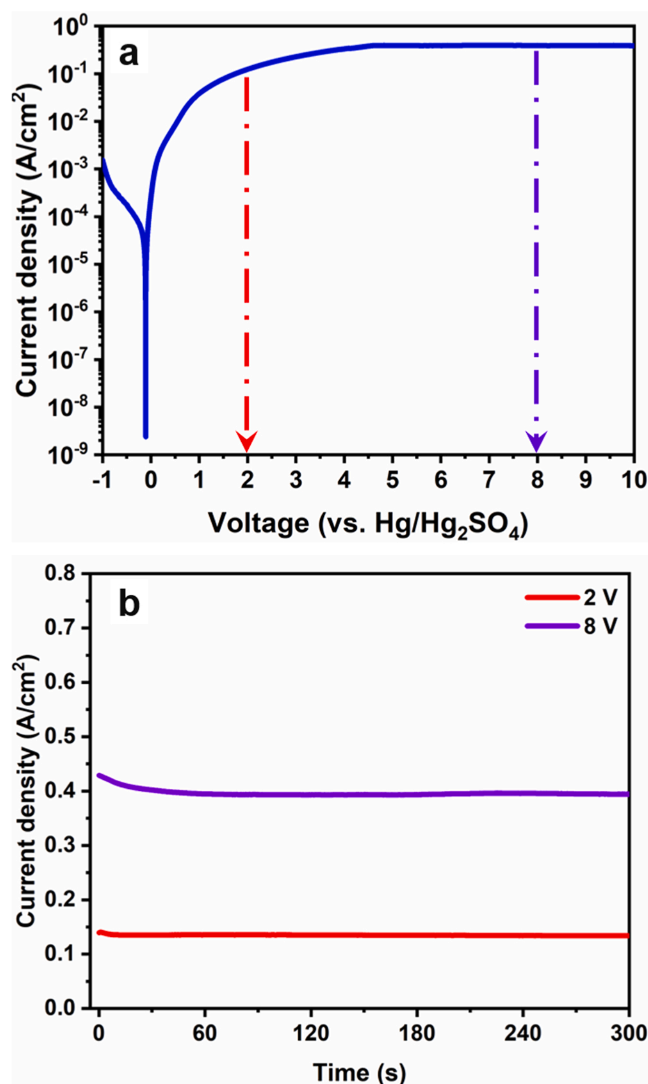

Fig. 1. (a) Polarization curve of tungsten in electrolyte with H_2SO_4 and methanol; (b) Chronoamperometry plots obtained at different voltages.

surface varies with crystal orientation, since the activation energies are different for different crystal planes, as mentioned by Ma et al. (2017). In the voltage range from 4.8 V to 10 V, the current density hardly changed with the voltage, indicating the mass transfer process has an influence on the dissolution of tungsten, therefore, the dissolution of tungsten is mass transfer polarization. In this region, the metal dissolution rate did not increase with voltage due to the accumulation of reaction products on the surface, thus, the mass transfer process is the rate-determining step of tungsten dissolution. As the electrolyte consisted of sulfuric acid and methanol, the mass transfer species probably is the tungsten cations. Piotrowski et al. (1998) mentioned that the transport of dissolved tetravalent titanium species from the anode surface to the bulk solution is rate-limiting during the electropolishing of titanium in sulfuric acid and methanol. It means that crystal planes with different orientations were dissolved at the limit rate of the mass transfer process. As Han and Fang (2019) suggested electropolishing can only be achieved under mass transfer polarization.

Chronoamperometry was performed to characterize the surface morphology evolution of tungsten. Fig. 1(b) shows the current-time curves obtained at applied voltages of 2 V, and 8 V. The curve obtained at a voltage of 2 V is almost unchanged. As the voltage of 2 V is in the range of the activation polarization region, the transfer of reactive products is fast and the surface concentration of reactive product did not differ appreciably from that of the bulk concentration. Therefore, no mass transfer effects existed, and the current density keep at constant as shown in the current-time curves. The curve obtained at the voltage of 8 V exhibited an obvious decreasing tendency in the early stage and then reached a plateau. The applied voltage of 8 V is in the range of mass transfer polarization region, therefore, the decreasing tendency in the current-time density was due to the gathering of the etching products, as discussed by Wang et al. (2019). Moreover, the drop of current density lasted for about 1 min before reaching the plateau, indicating that the accumulation of reactive products takes a certain time.

3.2. *Initial state of electropolishing*

The surface morphologies after etching for 1 s under the voltage of 2 V were shown in Fig. 2(a). Irregularly shaped etching pits were randomly distributed on the surface, and some of them were interconnected with adjacent pits. According to Tomashov and Chernova (1967), there is a passive film on the metal surface. Apparently, the formation of etching pits was due to the protective passivation film on the surface. The thickness of the passivation film spontaneously formed on tungsten was 0.97 nm, which was measured by the Elliptic partial instrument. Since the passivation film separated the underlying metal matrix from the electrolyte, the dissolution only occurred at the sites where the passivation film was broken down under the action of voltage, resulting in etching pits. The irregular shape of the etching pits indicated the etching was anisotropic under the activation polarization.

After etching for 5 min under the voltage of 2 V, the neighboring holes were merged, and the original surface was completely replaced by the etching pits, as shown in Fig. 2(b). Since the applied voltage of 2 V was in the activation polarization region, the dissolution rate varies with the crystal planes. Therefore, the dissolution of tungsten was anisotropic throughout the process. As shown in Fig. 2(e), the surface roughness was 490 nm after etching for 5 min. The applications of anisotropic etching on metal material have been reported by Yanagishita et al. (2017). It is suggested that porous Al particles prepared by anisotropic anodic etching of small Al particles are useful for various functional devices which require large surface area, such as substrates for catalysts and electrodes for electrolytic capacitors.

Similarly, irregularly shaped etching pits were formed on the surface after etching for 1 s under the voltage of 8 V, as shown in Fig. 2(c). The irregularly shaped etching pits indicated that the dissolution of tungsten in the early stage was anisotropic, although the applied voltage was within the mass transfer polarization region. Combining with the current-time curve under the voltage of 8 V, it can be inferred that it takes time to reach the stable mass transfer polarization state due to the accumulation of reactive products is time-consuming. However, the surface became flat after etching for 5 min under the voltage of 8 V, as shown in Fig. 2(d). There were obvious height differences between different grains on the flat surface due to the product layer was not thick enough. Similar grain boundary steps were reported by Guo et al. (2021) during the chemical mechanical polishing of tungsten alloy. The surface roughness of the flat surface was 74.4 nm as shown in Fig. 2(f). Those results implied that the mass transfer polarization is critical to achieving polishing effects, but it takes a certain time to enter the stable mass transfer polarization state.

3.3. *Transition of etching isotropy based on viscous layer*

According to the anodic dissolution behavior in the electrolyte with sulfuric acid and methanol, a transition process from activation polarization to mass transfer polarization existed during the electropolishing of tungsten under mass transfer polarization. In this set of experiments, the surface evolution during polishing was studied. Since the height difference between different crystal surfaces was still observed under the voltage of 8 V (vs. Hg/Hg_2SO_4), the polish of tungsten was conducted at the voltage of 30 V by using a DC power.

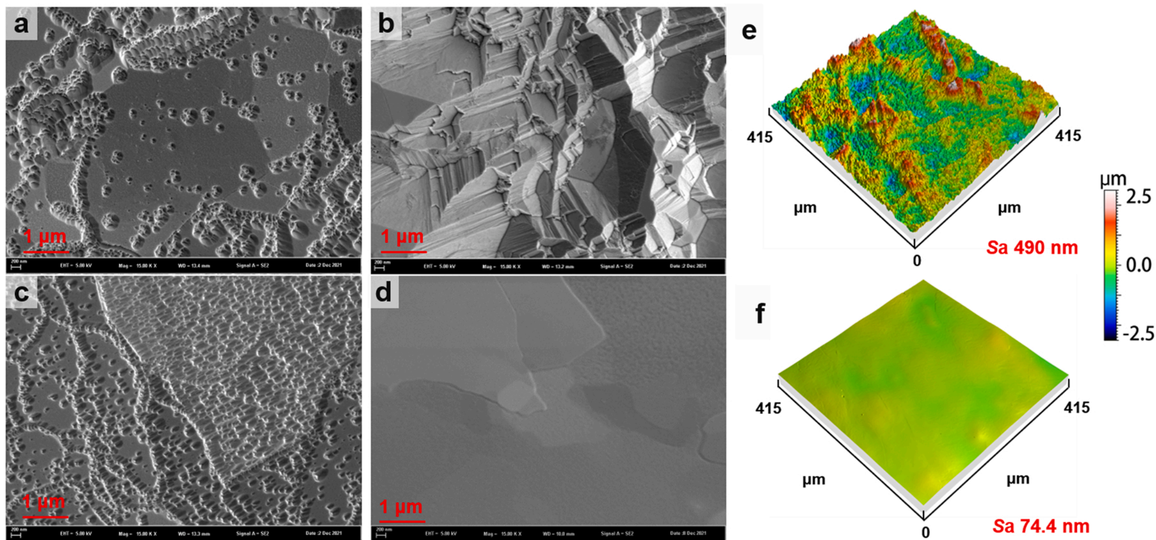

Fig. 2. Surface morphology and roughness observed by SEM and WLI under different etching conditions. (a) 1 s and (b, e) 5 min under the voltage of 2 V; (c) 1 s and (d, f) 5 min under the voltage of 8 V.

As shown in Fig. 3(a), the original substrate surface was smooth, and crystalline grain with different contrast could be observed clearly. After etching for 1 s, many small etching pits were randomly formed on the surface, and some basin structures were also formed on the surface because the etching pits merged together, as shown in Fig. 3(b). The bottom of the basin structures was rough due to the dissolution being orientation-dependent in the early stage. The nonetched residual area was reduced after etching for 3 s, as shown in Fig. 3(c). After etching for 5 s, the residual area was further reduced, only a few residual island-like areas were left on the surface. After etching for 10 s, the residual areas were completely removed, a smooth surface was obtained and crystalline grain with different contrast could be observed clearly again. It means that the accumulation of reactive products converted the dissolution of tungsten from activation polarization to mass transfer polarization. Finally, after etching for 120 s, the surface became significantly flat, as shown in Fig. 3(f). Apparently, the higher voltage promoted the accumulation of reactive products on the surface, the height difference between different crystal planes was not clear.

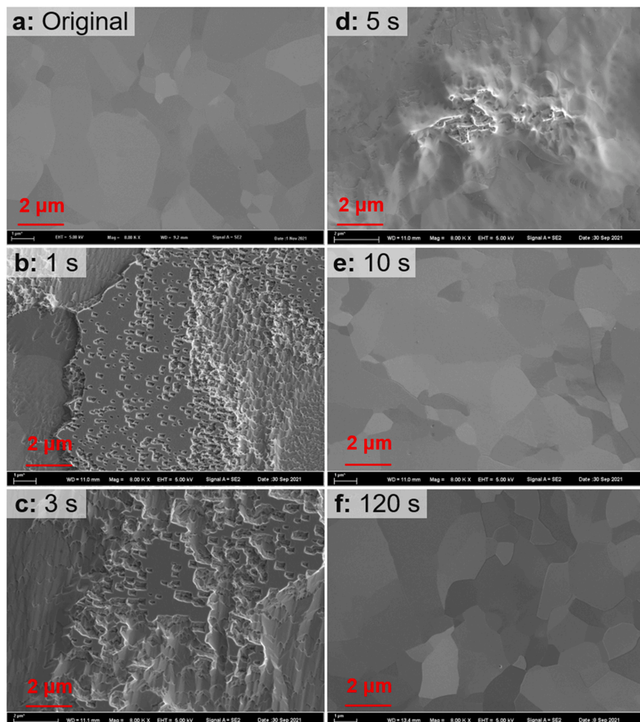

Fig. 3. Surface morphology evolution of tungsten during electropolishing observed by SEM.

Fig. 4 illustrates the surface roughness and current density variation during the polishing. Due to the generation of numerous etching pits, the Sa roughness increased first. After etching for 10 s, the Sa roughness decreased with increasing etching duration, which was attributed to the merging of the etching pits. The drastic drop in Sa roughness after 10 s was ascribed to the substrate surface was completely replaced by etching pits as shown in Fig. 3(e).

The current density showed a drastic drop in the early stage, then showed a fluctuation, and finally reached a plateau. The fluctuation in the range of 5–10 s was due to the growth of etching pits increasing the reactive area. The plateau means the dissolution entered the stable mass transfer polarization state, and surface polishing mainly occurred in the stage. The Sa roughness of the tungsten polished for 10 s and 2 min was 85 nm, and 5.56 nm respectively.

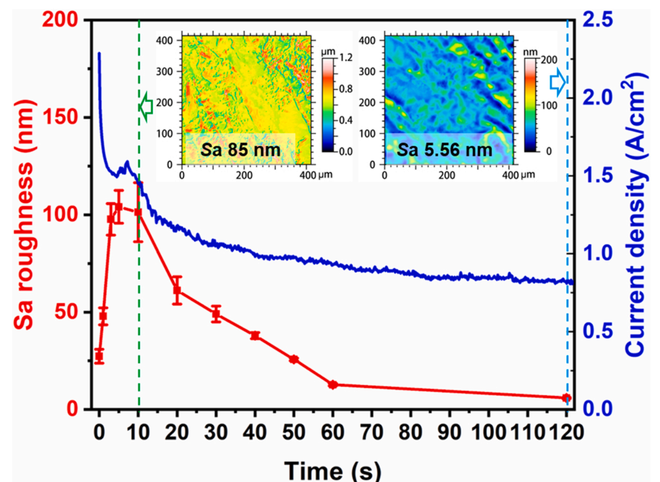

Fig. 4. Surface roughness and current-time curve during polishing.

3.4. Tuning of etching isotropy based on barrier layer

As previously discussed, surface polishing can be achieved under mass transfer polarization. Considering that the dissolution of metal under the mass transfer polarization is independent of crystal orientation, it is reasonable to expect the formation of isotropic etching pits during the electropolishing. Actually, the isotropic etching pit was not observed on the tungsten surface during the polishing, due to the thin thickness of the passivation film being removed before the mass transfer polarization was achieved. In order to observe the morphology of etching pits under the mass transfer polarization, the polished tungsten substrates were thermally oxidized at 350 ℃ for 0.5 h before the experiments. An oxide film of about 25 nm was formed on the surface. The polishing voltage was also 30 V.

As shown in Fig. 5(a), the original substrate surface was smooth. However, crystalline grain with different orientations cannot be distinguished due to the oxide film on the surface. After etching for 2 s, many small etching holes were randomly formed on the surface. Since the adjacent etching pits were interconnected, and the unshed passivation film was attached around the small etching pits, the shape of those etching pits was not a standard hemispherical, as shown in Fig. 5(b). After etching for 4 s, the etching pits were further merged to form a basin structure with a smooth bottom surface. After etching for 10 s, the residual area was further reduced, and individual etching pits of several microns in size can be observed, as shown in Fig. 5(d). Compared with the surface without oxidation, it takes longer for the entire surface to be completely replaced by the etching pits. From the top view, these etching pits were hemispherical. After etching for 30 s, only a few residual areas were left on the surface. Finally, after etching for 120 s, the surface became flat and the crystalline grain with different orientations can be distinguished. The surface profile of tungsten during polishing was shown in Fig. 5(g). Similarly, the roughness showed an increase at the early stage and then decreased. However, the roughness of the polished surface was larger than that of the original surface due to the oxide film blocking the dissolution of tungsten and reducing the efficiency of polishing.

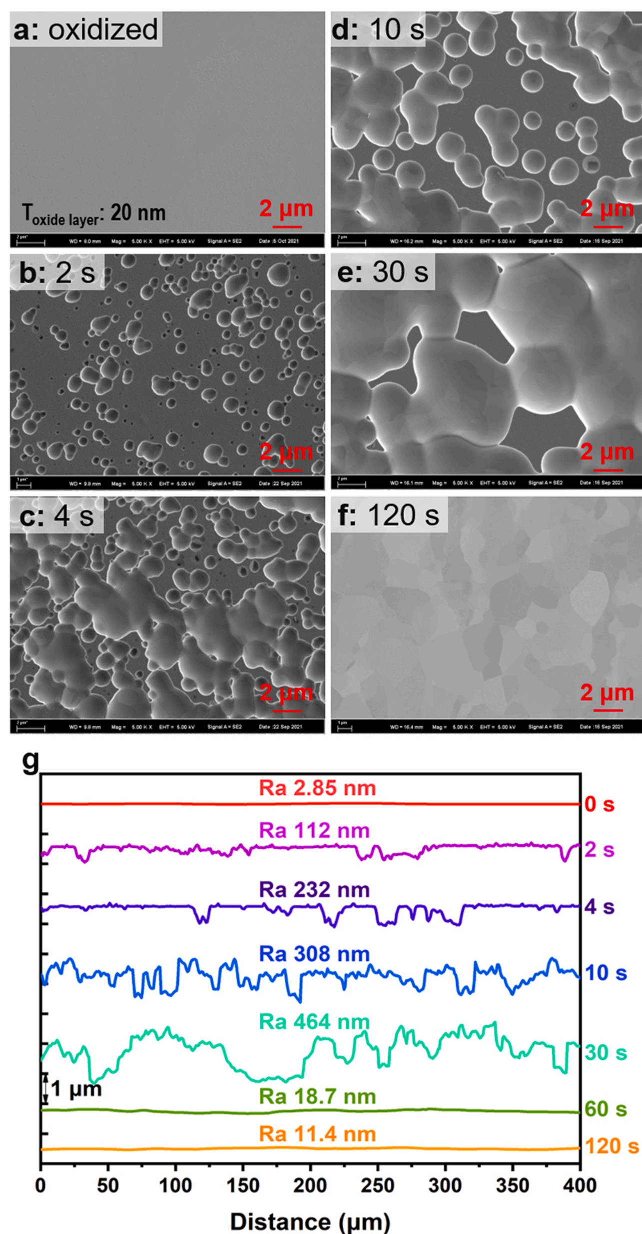

Fig. 5. Surface morphology evolution of thermal oxidized tungsten during polishing: (a-f) SEM morphology with different etching durations; and (g) surface profile and *Ra* roughness evolution during polishing.

As shown in Fig. 6, the etching pits formed on the tungsten after etching for 10 s with the voltage of 30 V were measured by AFM. As seen from Fig. 6(a), the etching pits were randomly distributed on the substrate surface, and some of them were interconnected with adjacent pits. The inner surface of a single etching pit with a diameter of about 2 μm was shown in Fig. 6(b), and the inner roughness was 0.757 nm. The insignificant Sa roughness value showed that the inner surface of the etching holes was smooth. Fig. 6(c) and (d) show the semicircular horizontal and vertical profiles of an etching hole from Fig. 6(a), indicating these etching pits were hemispherical. The isotropic etching pits formed during the electropolishing demonstrated that the dissolution of tungsten was independent of the crystal plane orientation under the mass transfer polarization. According to Madore and Landolt (1997), hemispherical etching pits with a diameter of 30 μm can be fabricated on a titanium surface at the mass transport limiting current density in the methanol electrolyte.

3.5. Tuning of etching isotropy based on pulse power supply

It was demonstrated that the mass transfer polarization takes time to achieve, due to the accumulation of the product layer. Therefore, it is important to keep the dissolution of the metal continuing to form a sufficient product layer.

As shown in Fig. 7, the tungsten substrates were etched at different duty cycles with the same pulse on duration. In order to ensure that the cumulative pulse-on time of each tungsten substrate was 1 min, the etching durations with a duty cycle of 80%, 50%, and 10% was 75 s, 120 s, and 600 s respectively.

As shown in Fig. 7(d) and (e), the tungsten surfaces were smooth after etching with the duty cycle of 80% and 50%. However, when the duty cycle was 10%, the tungsten surface became rough due to the etching being crystal surface orientation dependent. Since the pulse-on time was the same, the increase of pulse-off time prevented the accumulation of the product layer, thus the mass transfer polarization was hardly achieved, then resulting in the dissolution of tungsten was activation polarization. As mentioned by Yang et al. (2017), the pulse-off period facilitates replenishment of reacting species and removal of byproducts and heat. However, the duty cycle should be higher enough to make sure the formation of reactive products layer.

The surface evolution during the etching with a duty cycle of 10% was shown in Fig. 8(a)-(f). After etching for 1 s, the surface was distributed with small etching pits, as shown in Fig. 8(a). Since the etching pits were small, the shape was not clear. After etching for 3 s, anisotropic etching pits were observed on the surface. As the etching duration increased to 10 s, the etching pits covered the whole surface, as shown in Fig. 8(d). After etching for 30 s and 180 s, the dissolution of tungsten was still anisotropic, as shown in Fig. 8(e) and (f). The surface

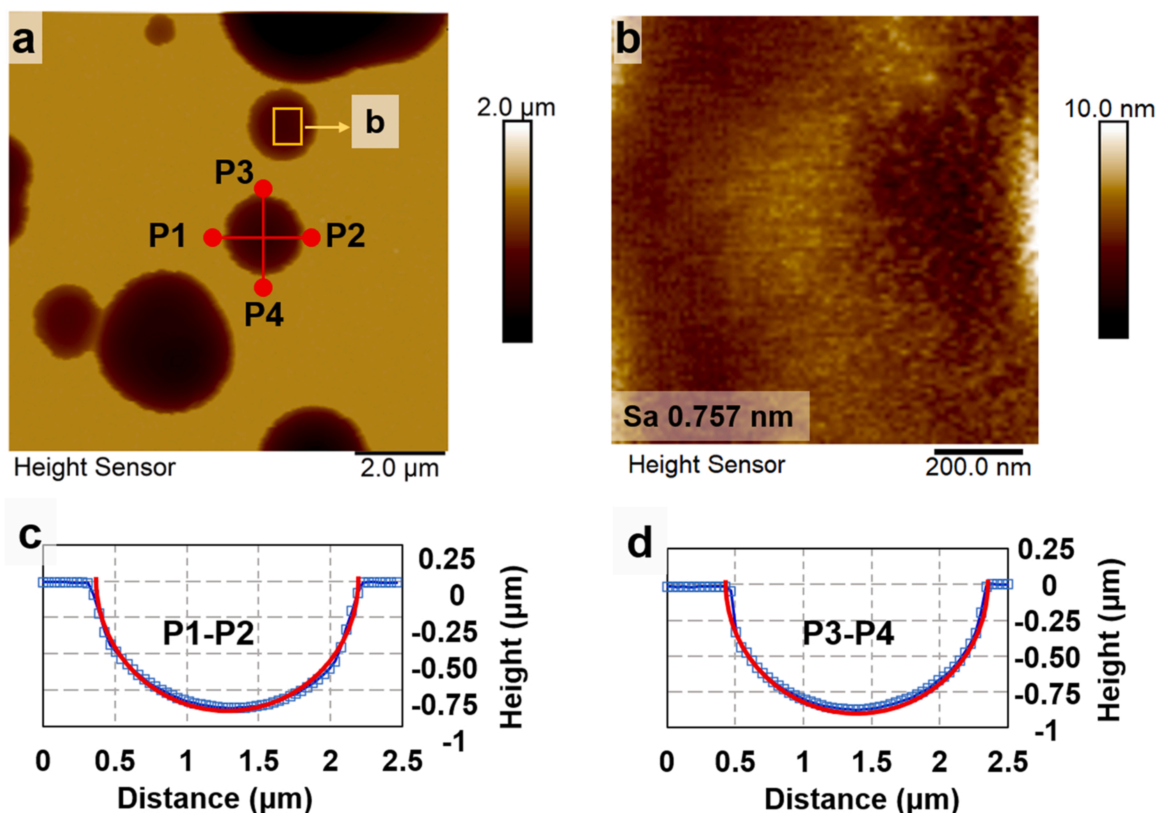

Fig. 6. Morphology of isotropic etching holes formed on tungsten measured by AFM: (a) overall morphology; (b) inner surface and (c, d) cross-sectional profiles of an etching pits.

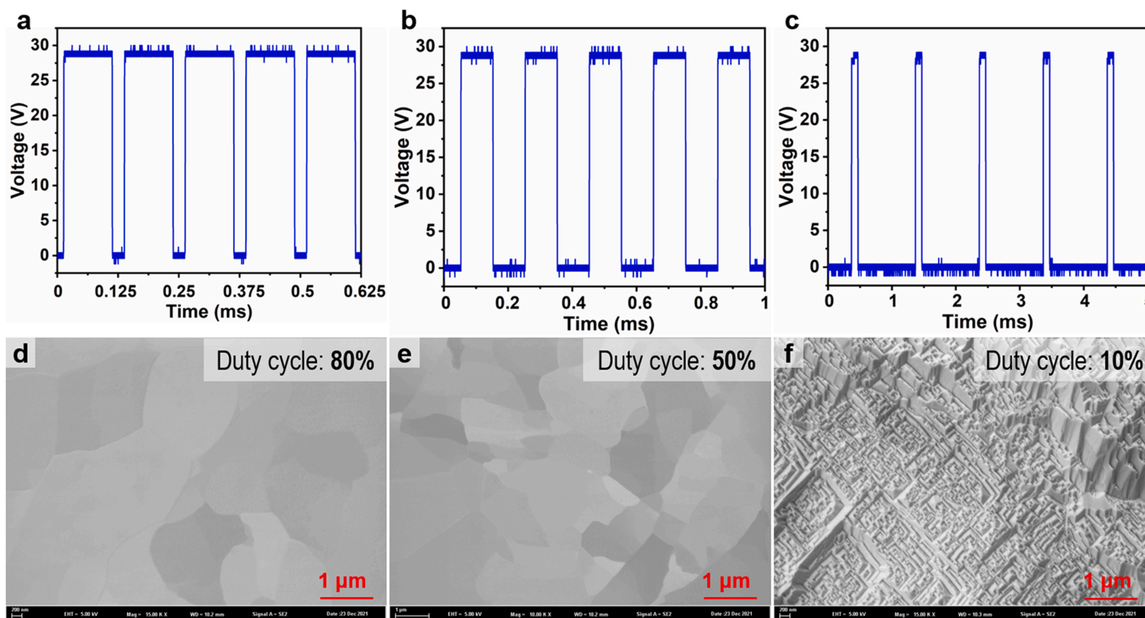

Fig. 7. The applied pulse voltage form and corresponding surface topography with pulse-on duration of 0.1 ms. (a, d) duty cycle of 80%, (b, e) duty cycle of 50%, (c, f) duty cycle of 10%.

morphology evolution during the dissolution process showed that the dissolution of tungsten cannot achieve mass transfer polarization because the pulse off time is much longer than the pulse on time. This is due to the fact that mass transfer continues during the pulse-off period of the pulse, while the charge transfer process of tungsten is suspended, so the reaction products cannot accumulate on the surface and the metal dissolution is always in an activated polarization state. As a result, the etching pits formed on the tungsten surface were anisotropic throughout the process.

The surface profile of tungsten during etching was shown in Fig. 8(g). The roughness showed an increasing tendency due to the anisotropic dissolution. The current density waveform was shown in Fig. 8(h). It is

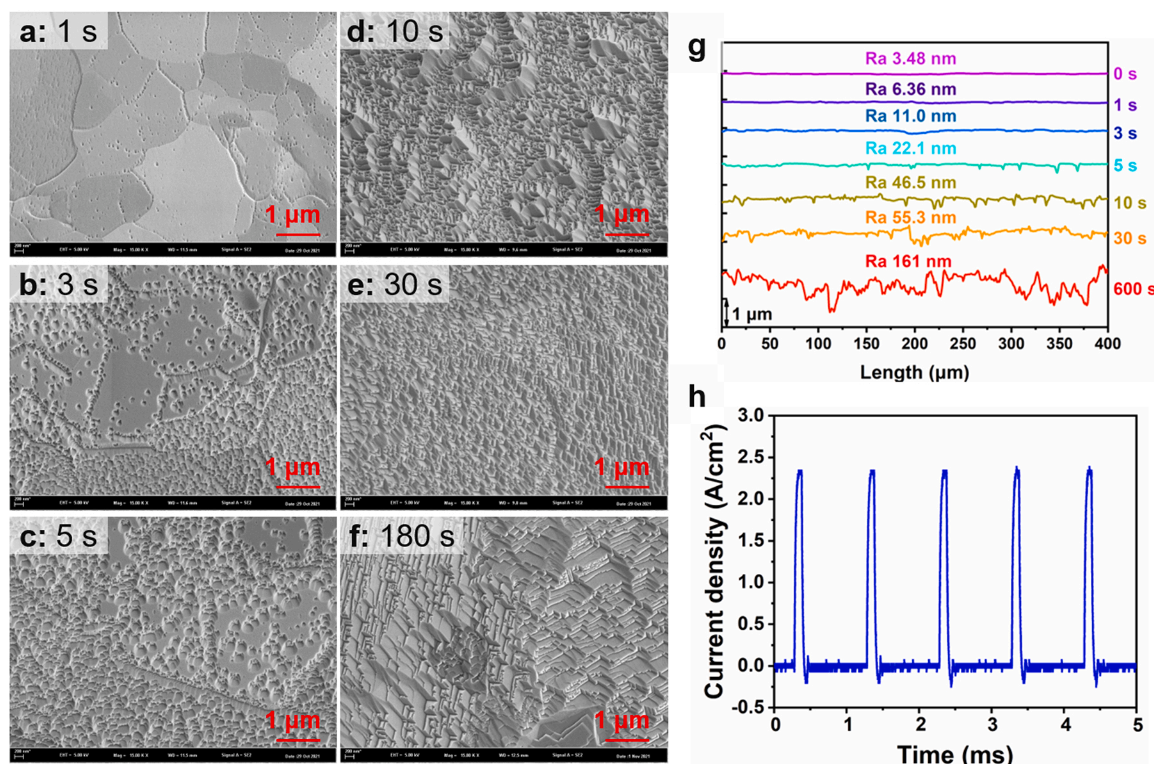

Fig. 8. Surface morphology evolution of tungsten during dissolution with duty cycle of 10%: (a-f) SEM images with different etching durations; (g) profile and *Ra* roughness evolution; (h) pulse current density waveform.

clear that the current density during the pulse-on time was 2.4 A/cm^2, which was larger than the stable current density obtained at the DC power as shown in Fig. 4. The high current density also demonstrated that the dissolution of tungsten was activation polarization.

3.6. Selection of electrolyte

Electrochemical etching of tungsten tips in NaOH electrolytes has drawn considerable attention as a highly efficient technique since the last decade. According to Qin and Deng (2019), an ultra-sharp nano--tungsten tip with a small radius of 5.5 nm, a long taper of 10 mm, and a large shank of 1 mm was obtained in the electrolyte composed of NaOH.

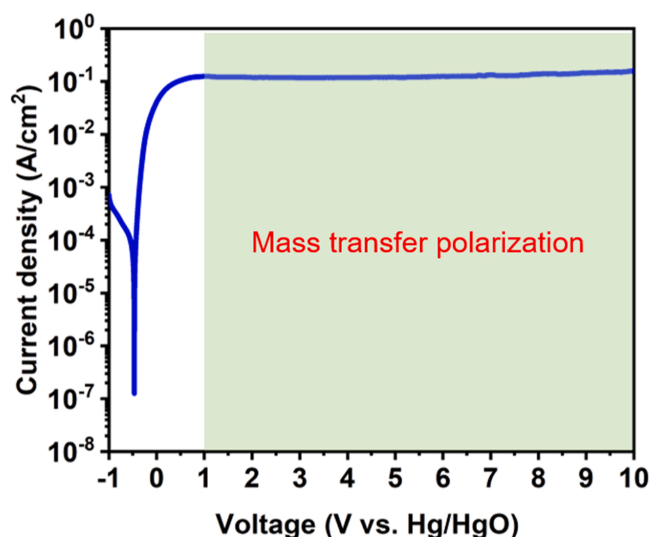

Fig. 9. Polarization curve of tungsten in the electrolyte with 2 wt% NaOH.

Therefore, the dissolution behavior of tungsten in 2 wt% NaOH was also investigated. Fig. 9 shows the polarization curve of tungsten in the electrolyte with 2 wt% NaOH, and it displayed a similar trend as shown in Fig. 1(a). In the anodic polarization region, when the voltage ranges from − 0.5 to 1 V, the current density increased with the voltage, indicating the dissolution of tungsten was activation polarization. Therefore, the dissolution of tungsten was anisotropic in this region. In the voltage range from 1 V to 10 V, the current density hardly changed with the voltage, indicating the dissolution of tungsten was mass transfer polarization. According to Han and Fang (2020b), the electropolishing effect is obtained in the limiting current density plateau region. Compared with the curve obtained in Fig. 1, the current density at the plateau region obtained in the electrolyte with 2 wt% NaOH was lower than that obtained in the electrolyte with H_2SO_4 and CH_3OH, and lower voltage was required to establish the mass transfer polarization in the electrolyte with NaOH. Different from the electrolyte with H_2SO_4 and methanol, the OH^- in the electrolyte prompted the formation of WO_3^{2-}, as mentioned by Anik and Osseo-Asare (2002). The negative charge of tungstate ion is easier to gather on the metal surface to form a product layer under the action of the electric field. Therefore, the mass transfer polarization was easier to obtain in the electrolyte with NaOH.

Chronoamperometry plots of tungsten under different voltages in the electrolyte with 2 wt% NaOH were shown in Fig. 10(a). At the voltage of 0.2 V, which was in the activation polarization region, the current density was almost unchanged over time. At the voltage of 5 V, which was in the mass transfer polarization region, the current-time curve exhibited a sharp decreasing tendency in the early stage and then reached a plateau. The sharply decreasing trend of the current density-time curve indicated a strong aggregation effect of the dissolving products on the surface.

The surface morphologies after etching for 1 s under the voltage of 0.2 V and 5 V were shown in Fig. 10(b) and (d). Irregularly shaped etching pits were randomly distributed on those two surfaces, and some of the etching pits were interconnected with adjacent pits. Those

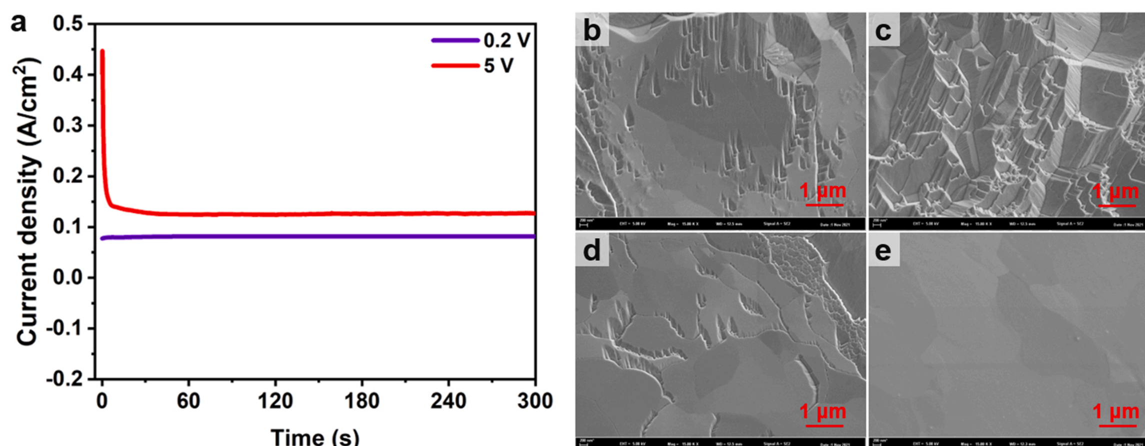

Fig. 10. (a) Chronoamperometry plots obtained at different voltages; Surface morphology after etching for (b) 1 s and (c) 5 min under the voltage of 2 V; and after etching for (d) 1 s and (e) 5 min under the voltage of 5 V.

irregular shapes of etching pits indicated that the dissolution of tungsten was anisotropic at the early stage, regardless of whether the voltage applied was in the active polarization region or in the mass transfer polarization region. After etching for 5 min at the voltage of 0.2 V, the original surface was completely covered with etching pits. Since the voltage of 0.2 V was in the activation polarization region, the dissolution of tungsten was anisotropic, so the surface was rough after dissolution for 5 min as shown in Fig. 10(c). However, after etching for 5 min at the voltage of 5 V, the tungsten surface became flat, as shown in Fig. 10(e). This set of experiments also demonstrated the electropolishing of tungsten can only be achieved under mass transfer polarization.

According to the polarization curve, the tungsten can be polished at a voltage of larger than 1 V (vs. Hg/HgO) in the electrolyte with 2 wt% NaOH. In order to get a smooth surface, the polishing of tungsten was conducted under the voltage of 10 V with a DC power supply.

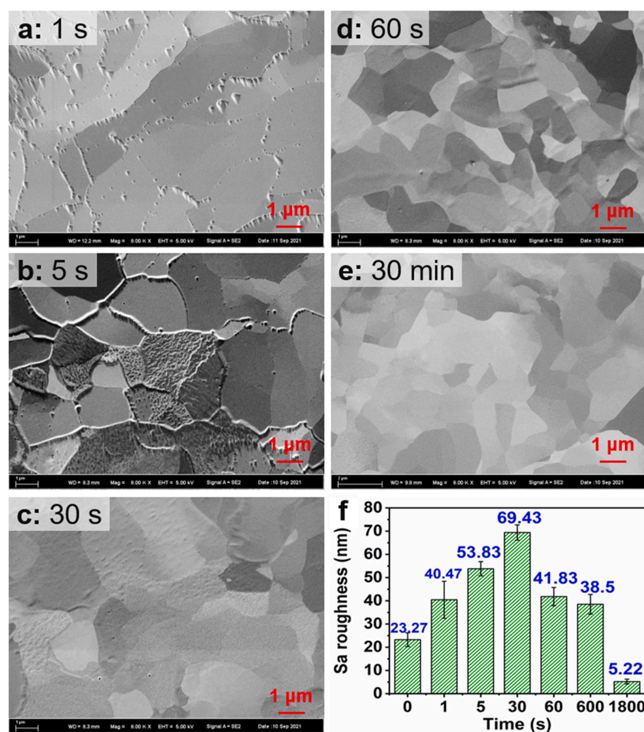

Fig. 11. Surface morphology evolution of tungsten during dissolution (a-e) SEM images with different polishing durations; and (f) *Sa* roughness value versus time.

As shown in Fig. 11(a), after polishing for 1 s, the surface was distributed with anisotropic etching pits, and these etching pits preferentially formed on the grain boundary due to the weak protective effect of the thin passivation film on the surface. The intergranular corrosion of high purity nickel in H_2SO_4 was mentioned by Palumbo and Aust (1990) and the corrosion morphology was potential-dependent. After etching for 5 s, the etching pits were connected with adjacent pits to form a complex surface topography, as shown in Fig. 11(b), which indicated that the dissolution of tungsten was activation polarization. After etching for 30 s, the edge of the complex structures previously formed became blurred, indicating the transformation of tungsten dissolution from activation polarization to mass transfer polarization due to the accumulation of reactive products, as shown in Fig. 11(c). After etching for 60 s, a smooth surface was obtained while minute signs of waviness could be observed. Finally, after etching for 30 min, the surface became significantly flat, as shown in Fig. 11(e).

Fig. 11(f) shows the Sa roughness of the tungsten substrate after etching for different durations. The Sa roughness increased first and then decreased with increasing etching duration. The increasing Sa roughness was the consequence of the generation of etching pits, while the decrease in the Sa roughness was attributed to the establishment of a stable mass transfer polarization state. After polishing for 30 min, the Sa roughness was 5.22 nm. Since the current density plateau on the polarization curve in the electrolyte with NaOH was lower than in the electrolyte with H_2SO_4, electropolishing of tungsten in NaOH takes longer to achieve the same effect.

As shown in Fig. 12, the tungsten substrates were etched at different duty cycles with the same pulse-on time. In order to ensure that the cumulative pulse-on time of each tungsten substrate was 1 min, the etching durations with a duty cycle of 50%, 10%, and 1% was 120 s, 600 s, and 6000 s respectively.

As shown in Fig. 12(d) and (e), the tungsten surfaces were smooth after etching with the duty cycle of 50% and 10%. Until the duty cycle decreased to 1%, the tungsten surface became rough, as shown in Fig. 12 (f). Similar to the results obtained in the electrolyte with H_2SO_4 and CH_3OH, the increase of pulse-off time prevented the accumulation of product layer, then resulting in the dissolution of tungsten was anisotropic all the time. As discussed by Ju et al. (2009), high-quality probes with ultra-smooth surfaces can be achieved with the proper combination of pulse current and electrolyte concentration.

The surface evolution during the etching with a duty cycle of 1% was shown in Fig. 13(a)-(f). After etching for 1 s, the surface was distributed with anisotropic etching pits, as shown in Fig. 13(a). There was also a preferentially etching around the grain boundary. After etching for 5 s, the etching pits connected with adjacent pits. As the etching duration increased to 10 s, the unetched area further reduced, as shown in Fig. 13

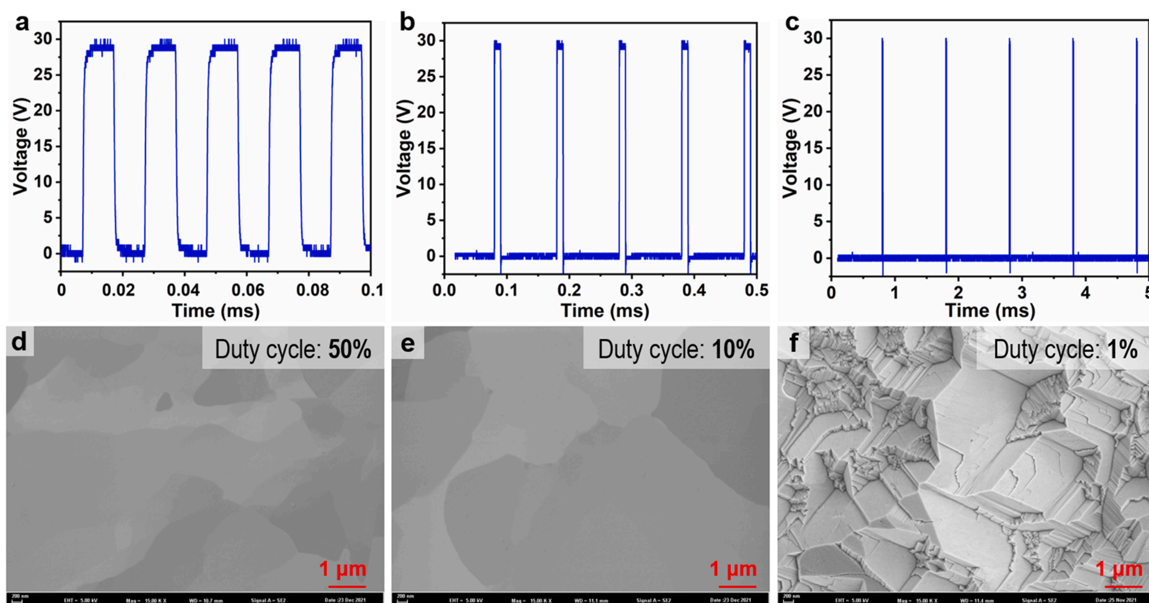

Fig. 12. The applied pulse voltage form and corresponding surface topography with pulse-on duration of 0.01 ms. (a, d) duty cycle of 50%, (b, e) duty cycle of 10%, (c, f) duty cycle of 1%.

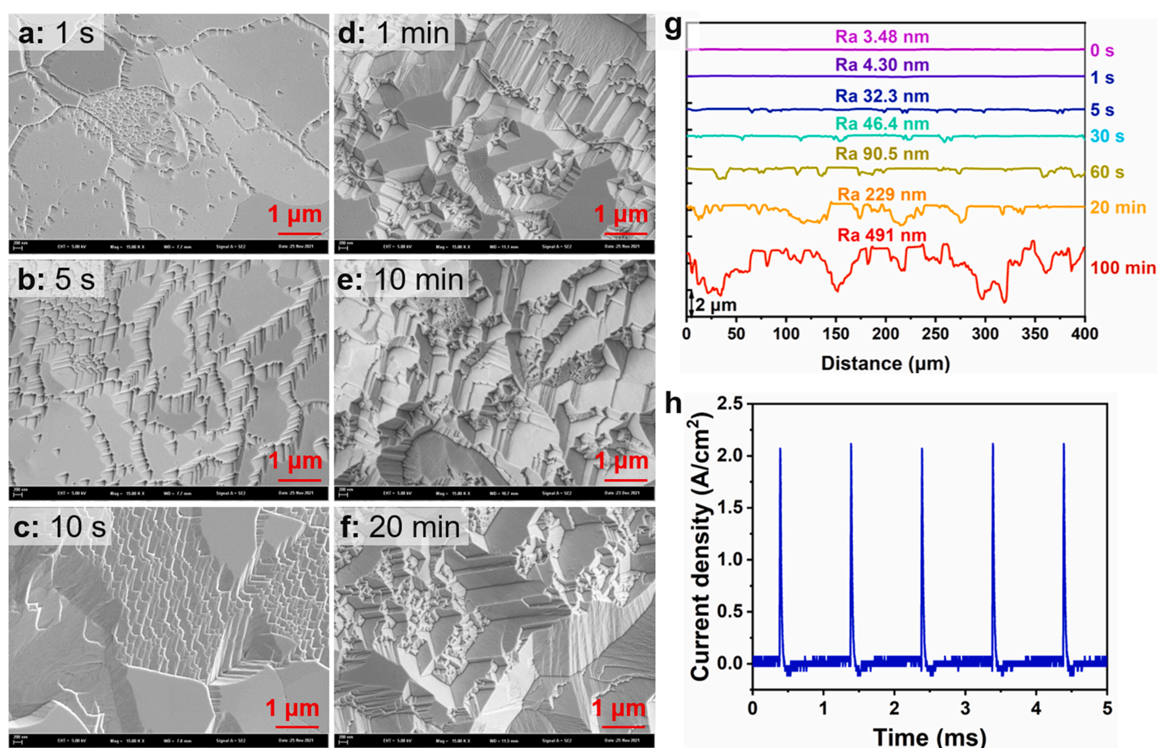

Fig. 13. Surface morphology evolution of tungsten during dissolution with duty cycle of 1%: (a-f) SEM morphology with different etching durations; (g) profile and *Ra* roughness evolution; (h) pulse current density waveform.

(c). After etching for 1 min, the dissolution of tungsten was still anisotropic, as shown in Fig. 13(d). After etching for 10 min and 20 min, the whole surface started to dissolve. Due to the dissolution being anisotropic, the surface morphology was complex, as shown in Fig. 13(e) and (f). Since the mass transfer continued during the pulse-off time while the oxidation of tungsten was suspended, the dissolution of tungsten was always anisotropic during the dissolution process.

The surface profile of tungsten during etching was shown in Fig. 13 (g). The roughness showed an increasing tendency due to the dissolution of tungsten being anisotropic. The current density waveform was shown in Fig. 13(h). The current density during the pulse-on time was about 2.2 A/cm^2. The high current density under the pulse power supply implied a higher dissolution rate of tungsten despite the rough surface. Similar conclusions were obtained in the fabrication of the tungsten microelectrodes. Fan et al. (2010) suggested that a pulsed power supply in fabricating the microelectrode can increase mass diffusion, reduce concentration polarization, and increase the machining removal rate.

4. Anodic dissolution model of tungsten

The existing theories, such as viscous layer theory, diffusion theory, and passivation theory, emphasize the importance of the mass transfer for electropolishing, although the species been transferred are different, as summarized by Lyczkowska-Widlak et al. (2020). This has also been confirmed by the electrochemical dissolution behaviors of tungsten in NaOH and H_2SO_4-CH_3OH electrolytes. Combining the aforementioned theories with the dissolution behaviors of tungsten, the electropolishing of tungsten usually consisted of four stages: anisotropic etching stage, isotropic etching stage, pits merging stage, and surface leveling stage, as depicted in Fig. 14.

At the first stage, the weak sites of the passivation film break down under the action of the electric field. And the tungsten grains dissolves at those breakdown sites. Due to the low concentration of the reaction product, it is not sufficient to form a thick product layer around the breakdown sites. Therefore, the dissolution of tungsten is in the activation polarization state, resulting in anisotropic etching pits on the surface. The surface roughness shows an increase in this stage, owing to the presence of irregular etching pits. This process is regarded as the anisotropic etching stage.

At the second stage, due to the growth of the previously formed etching pits, sufficient reaction products accumulate inside the etching pits and form a thick enough product layer, thus, the dissolution of tungsten enters the mass transfer polarization stage and isotropic etching pits with regular hemispheric shape are formed.

With the growth of the isotropic etching pits, they merge together and the passivation film falls off and the initial rough surface is completely replaced by the pit-merged fresh surface. This is the pit-merging stage and a smooth surface could be obtained under the suitable conditions of IEP.

At the fourth stage, a thick layer of reactive products formed on the surface, indicating that the dissolution of tungsten is dominated by mass transfer process. Depending on the electrolyte composition used, the reaction product layer can be either tungsten cations or tungstate ions. Surface leveling mainly occurs at this stage and the surface becomes smooth.

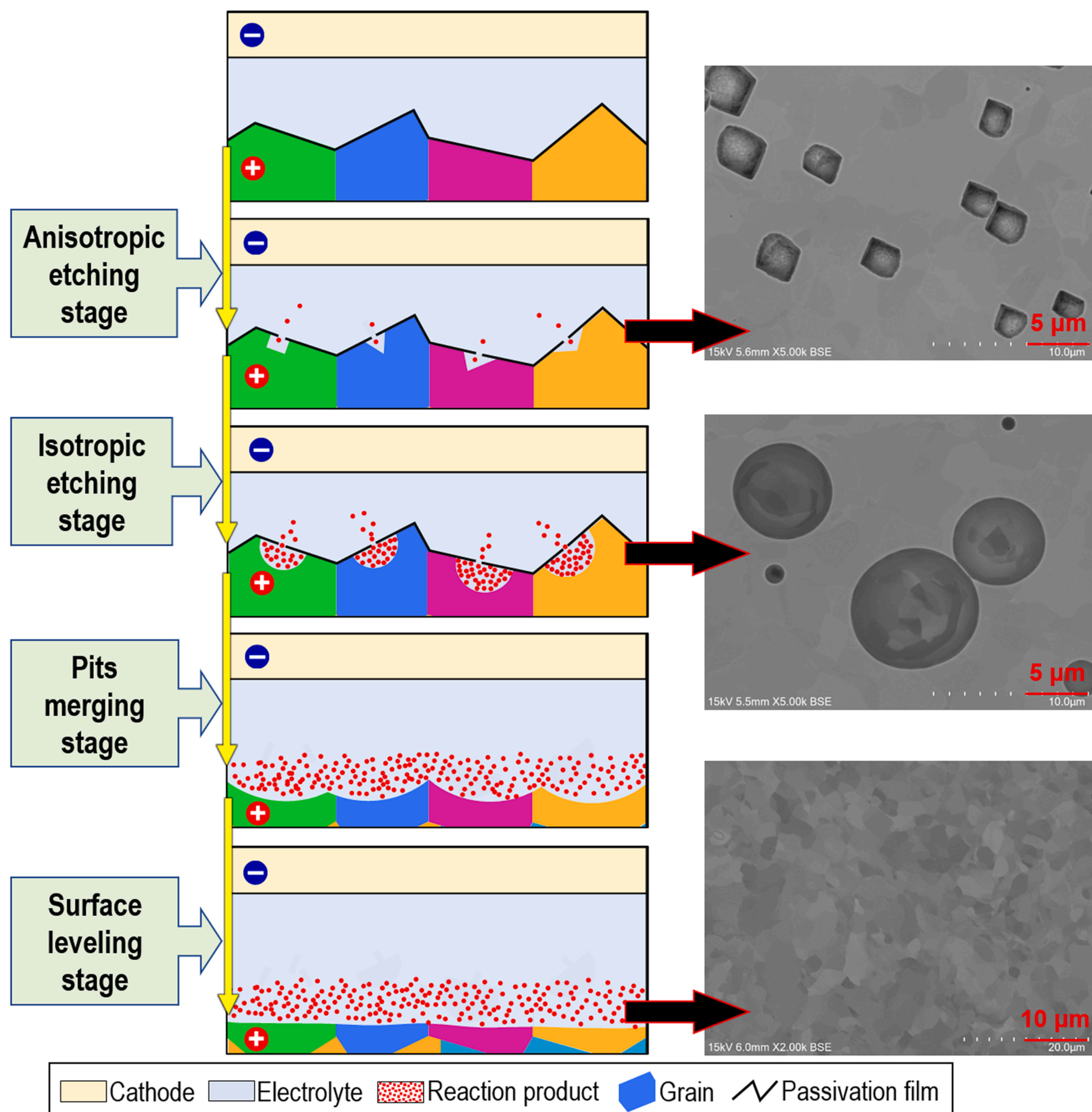

Fig. 14. The sketch map for the evolution of the dissolution process of tungsten.

5. Conclusion

In this paper, the mechanism of electropolishing of tungsten was comprehensively studied from the perspective of etching isotropy. To summarize, the following conclusions can be drawn from this study:

- The anodic dissolution of tungsten consists of an activation polarization region and a mass transfer polarization region in despite of the electrolyte composition. And the electropolishing can only be achieved under mass transfer polarization.
- The initial stage of tungsten dissolution is always anisotropic. With the accumulation of reaction products, the mass transfer polarization can be realized and the surface will be smoothed.
- Based on the dissolution behaviors of tungsten, the electropolishing of tungsten usually consisted of four stages: anisotropic etching, isotropic etching, pits merging, and surface leveling.
- For electropolishing using H_2SO_4-CH_3OH (3:20 volume ratio), the mass transfer polarization can be achieved as the voltage is larger than 4.8 V (vs. Hg/Hg_2SO_4) with a corresponding current density of 0.81 A/cm^2. The *S*a roughness decreased from 28.2 nm to 5.56 nm for 2 min of electropolishing (30 V).
- For electropolishing using 2 wt% NaOH, the mass transfer polarization can be achieved as the voltage larger than 1 V (vs. Hg/HgO) with a corresponding current density of 0.13 A/cm^2. The surface *S*a roughness decreased from 23.27 nm to 5.22 nm for 30 min of electropolishing (10 V).

Electropolishing is an old and widely utilized technique with numerous reports on its mechanisms. However, the etching isotropy during electropolishing is seldom studied. It has been revealed that, regardless of electrolyte composition, current density, pulse duty cycle and other parameters, isotropic etching under mass transfer polarization plays the key role for surface smoothing via electropolishing. This paper provides new insights into the intrinsic mechanism of electropolishing. For the practical applications of electropolishing towards different metals or alloys, the etching isotropy may be a more direct and efficient criteria for process development.

CRediT authorship contribution statement

Rong Yi: Data curation, Conceptualization, Methodology, Writing - original draft. **Jianwei Ji:** Data curation, Validation **Zejin Zhan:** Data curation, Methodology. **Hui Deng:** Conceptualization, Methodology. Project administration, Supervision.

Declaration of Competing Interest

The authors declare the following financial interests/personal relationships which may be considered as potential competing interests: Hui Deng reports financial support was provided by National Natural Science Foundation of China.

Acknowledgments

This project is supported by the National Natural Science Foundation of China (52005243, 52035009) and the Science and Technology Innovation Committee of Shenzhen Municipality (JCYJ20200109141003910, JCYJ20210324120402007). The authors acknowledge the assistance of SUSTech Core Research Facilities.

References

Anik, M., Osseo-Asare, K., 2002. Effect of pH on the anodic behavior of tungsten. J. Electrochem. Soc. 149, B224.
Aspinwall, D.K., Soo, S.L., Berrisford, A.E., Walder, G., 2008. Workpiece surface roughness and integrity after WEDM of Ti–6Al–4V and Inconel 718 using minimum damage generator technology. CIRP Ann. 57, 187–190.
Bard, A., Faulkner, L., 2002. Electrochemical Methods: Fundamentals and Applications.
Chen, H.-C., Lin, J.-C., Yang, Y.-K., Tsai, C.-H., 2010. Optimization of wire electrical discharge machining for pure tungsten using a neural network integrated simulated annealing approach. Expert Syst. Appl. 37, 7147–7153.
Di, M., Li, S., Liang, C., 2009. Electropolishing of high-purity aluminium in perchloric acid and ethanol solutions. Corros. Sci. 51, 713–718.
Elmore, W.C., 1939. Electrolytic polishing. J. Appl. Phys. 10, 724–727.
Fan, Z.-W., Hourng, L.-W., Wang, C.-Y., 2010. Fabrication of tungsten microelectrodes using pulsed electrochemical machining. Precis. Eng. 34, 489–496.
Ferchow, J., Hofmann, U., Meboldt, M., 2020. Enabling electropolishing of complex selective laser melting structures. Procedia CIRP 91, 472–477.
Guo, J., Shi, X., Song, C., Niu, L., Cui, H., Guo, X., Tong, Z., Yu, N., Jin, Z., Kang, R., 2021. Theoretical and experimental investigation of chemical mechanical polishing of W–Ni–Fe alloy. Int. J. Extrem. Manuf. 3.
Halfawy, M., 1951. On the theory of electrolytic polishing. Experientia 7, 175–176.
Han, W., Fang, F., 2019. Fundamental aspects and recent developments in electropolishing. Int. J. Mach. Tools Manuf. 139, 1–23.
Han, W., Fang, F., 2020a. Eco-friendly NaCl-based electrolyte for electropolishing 316L stainless steel. J. Manuf. Process. 58, 1257–1269.
Han, W., Fang, F.Z., 2020b. Investigation of electropolishing characteristics of tungsten in eco-friendly sodium hydroxide aqueous solution. Adv. Manuf. 8, 265–278.
Hoar, T.P., Mears, D.C., Rothwell, G.P., 1965. The relationships between anodic passivity, brightening and pitting. Corros. Sci. 5, 279–289.
Ionov, A.M., Chekmazov, S.V., Usov, V., Nesterova Mcapital Ie, C., Aronin, A.S., Semenov, V.N., Shvets, I.V., Bozhko, S.I., 2020. Deformation and fracture of crystalline tungsten and fabrication of composite STM probes. Ultramicroscopy 218, 113083.
Jacquet, P.A., 1935. Electrolytic method for obtaining bright copper surfaces. Nature 135, 1076.
Jiang, G., Jianguo, Z., Yanan, P., Renke, K., Yoshiharu, N., Paul, S., Xiaobin, Y., Baorui, W., Dongming, G., 2020. A critical review on the chemical wear and wear suppression of diamond tools in diamond cutting of ferrous metals. Int. J. Extrem. Manuf. 2.
Ju, B.-F., Chen, Y.-L., Fu, M., Chen, Y., Yang, Y., 2009. Systematic study of electropolishing technique for improving the quality and production reproducibility of tungsten STM probe. Sens. Actuators A Phys. 155, 136–144.
Landolt, D., 1987. Fundamental aspects of electropolishing. Electrochim. Acta 32, 1–11.
Landolt, D., Chauvy, P.F., Zinger, O., 2003. Electrochemical micromachining, polishing and surface structuring of metals: Fundamental aspects and new developments. Electrochim. Acta 48, 3185–3201.
Lyczkowska-Widlak, E., Lochynski, P., Nawrat, G., 2020. Electrochemical polishing of austenitic stainless steels. Materials 13.
Ma, H., Chen, X.-Q., Li, R., Wang, S., Dong, J., Ke, W., 2017. First-principles modeling of anisotropic anodic dissolution of metals and alloys in corrosive environments. Acta Mater. 130, 137–146.
Madore, C., Landolt, D., 1997. Electrochemical micromachining of controlled topographies on titanium for biological applications. J. Micromech. Microeng. 7, 270.
Magaino, S., Matlosz, M., Landolt, D., 1993. An impedance study of stainless steel electropolishing. J. Electrochem. Soc. 140, 1365–1373.
Matlosz, M., Magaino, S., Landolt, D., 1994. Impedance analysis of a model mechanism for acceptor-limited electropolishing. J. Electrochem. Soc. 141, 410–418.
Muhammad Ajmal, K., Yi, R., Zhan, Z., Ji, J., Zhang, X., Deng, H., 2021. Highly efficient smoothing of Inconel 718 via electrochemical-based isotropic etching polishing. Precis. Eng. 71, 119–129.
Neelakantan, L., Hassel, A.W., 2008. Rotating disc electrode study of the electropolishing mechanism of NiTi in methanolic sulfuric acid. Electrochim. Acta 53, 915–919.
Palumbo, G., Aust, K., 1990. Structure-dependence of intergranular corrosion in high purity nickel. Acta Metall. Mater. 38, 2343–2352.
Philipps, V., 2011. Tungsten as material for plasma-facing components in fusion devices. J. Nucl. Mater. 415, S2–S9.
Piotrowski, O., Madore, C., Landolt, D., 1998. The mechanism of electropolishing of titanium in methanol-sulfuric acid electrolytes. J. Electrochem. Soc. 145, 2362–2369.
Puri, A.B., Bhattacharyya, B., 2003. An analysis and optimisation of the geometrical inaccuracy due to wire lag phenomenon in WEDM. Int. J. Mach. Tools Manuf. 43, 151–159.
Qin, S., Deng, H., 2019. Electrochemical etching of tungsten for fabrication of sub-10-nm tips with a long taper and a large shank. Nanomanuf. Metrol. 2, 235–240.
Ren, C., Fang, Z.Z., Koopman, M., Butler, B., Paramore, J., Middlemas, S., 2018. Methods for improving ductility of tungsten - A review. Int. J. Refract. Metals Hard Mater. 75, 170–183.
Rieth, M., Dudarev, S.L., Gonzalez de Vicente, S.M., Aktaa, J., Ahlgren, T., Antusch, S., Armstrong, D.E.J., Balden, M., Baluc, N., Barthe, M.F., Basuki, W.W., Battabyal, M., Becquart, C.S., Blagoeva, D., Boldyryeva, H., Brinkmann, J., Celino, M., Ciupinski, L., Correia, J.B., De Backer, A., Domain, C., Gaganidze, E., García-Rosales, C., Gibson, J., Gilbert, M.R., Giusepponi, S., Gludovatz, B., Greuner, H., Heinola, K., Höschen, T., Hoffmann, A., Holstein, N., Koch, F., Krauss, W., Li, H., Lindig, S., Linke, J., Linsmeier, C., López-Ruiz, P., Maier, H., Matejicek, J., Mishra, T.P., Muhammed, M., Muñoz, A., Muzyk, M., Nordlund, K., Nguyen-Manh, D., Opschoor, J., Ordás, N., Palacios, T., Pintsuk, G., Pippan, R., Reiser, J., Riesch, J., Roberts, S.G., Romaner, L., Rosiński, M., Sanchez, M., Schulmeyer, W., Traxler, H., Ureña, A., van der Laan, J.G., Veleva, L., Wahlberg, S., Walter, M., Weber, T., Weitkamp, T., Wurster, S., Yar, M.A., You, J.H., Zivelonghi, A., 2013. Recent progress in research on tungsten materials for nuclear fusion applications in Europe. J. Nucl. Mater. 432, 482–500.

Sachs, J., 1999. Metal Prices in the United States through 1998.

Suzuki, N., Haritani, M., Yang, J., Hino, R., Shamoto, E., 2007. Elliptical vibration cutting of tungsten alloy molds for optical glass parts. CIRP Ann. 56, 127–130.

Tomashov, N.D., Chernova, G.P., 1967. The phenomenon of passivity in metals. Passivity and Protection of Metals Against Corrosion. Springer, US, Boston, MA, pp. 9–53.

Wang, F., Zhang, X., Deng, H., 2019. A comprehensive study on electrochemical polishing of tungsten. Appl. Surf. Sci. 475, 587–597.

Wang, J., Chen, W., Han, F., 2014. Study on the magnetorheological finishing method for the WEDMed pierced die cavity. Int. J. Adv. Manuf. Technol. 76, 1969–1975.

Wynick, G., Boehlert, C., 2005. Use of electropolishing for enhanced metallic specimen preparation for electron backscatter diffraction analysis. Mater. Charact. 55, 190–202.

Yanagishita, T., Imaizumi, M., Kondo, T., Masuda, H., 2017. Formation of porous Al particles by anisotropic anodic etching. Electrochem. Commun. 78, 26–28.

Yang, G., Wang, B., Tawfiq, K., Wei, H., Zhou, S., Chen, G., 2017. Electropolishing of surfaces: theory and applications. Surf. Eng. 33, 149–166.

Yi, R., Zhang, Y., Zhang, X., Fang, F., Deng, H., 2020. A generic approach of polishing metals via isotropic electrochemical etching. Int. J. Mach. Tools Manuf. 150.